Archives of Acoustics Vol. 50, No. 2, pp. 277–288 (2025), https://doi.org/10.24425/aoa.2025.153665

Research Paper

Aeroacoustic Effect of Savonius Rotor Segmentation

Shivangi SACHAR(1)*, Piotr DOERFFER(1), Paweł FLASZYŃSKI(1), Józef KOTUS(2)a, Krzysztof DOERFFER(2), Joanna GRZELAK(2), Michał PIOTROWICZ(1)

(1) *Institute of Fluid Flow Machinery, Polish Academy of Sciences*
Gdańsk, Poland

(2) *Gdańsk University of Technology*
[a] *Faculty of Electronics, Telecommunications and Informatics, Audio Acoustics Laboratory*
Gdańsk, Poland

*Corresponding Author e-mail: shivangi_sachar@hotmail.com

Received February 24, 2025; revised April 10, 2025; accepted April 10, 2025; published online June 6, 2025.

Switching to renewable energy has been accelerated in recent decades due to the depleting fossil fuel reserves and the need to mitigate environmental and climate degradation. Wind power, especially in urban areas, has seen a significant growth. A critical consideration in the urban wind turbine installation is the noise impact on residents. This study investigates the noise generated by wind turbines under different operational conditions, comparing single-segment and five-segment rotor designs. Various acoustic analyses were conducted, including broadband analysis with weighting curves Z, A, C, and G, a narrowband analysis using 1/12 octave bands, and broadband calculations of sound quality indicators such as sharpness, roughness, and fluctuation strength (FS). The FS was also examined in the Bark scale frequency domain. The study linked the acoustic analysis with the rotor efficiency related to power production. The findings indicate that five-segment rotors generate less acoustic energy due to phase shifts, enhancing dissipation rates, and acoustic energy decreases with the increasing load, peaking when rotors are free at high revolutions per minute (RPM). While single-segment rotors show higher efficiency, they produce more noise. In contrast, five-segment rotors offer a better sound quality, making them preferable despite a lower efficiency. This research provides essential insights into designing urban wind turbines that balance efficiency and noise, crucial for sustainable energy solutions.

Keywords: wind power; wind turbines; rotor efficiency; Savonius rotor segmentation.

1. Introduction

Noise from wind turbines is a significant concern in energy production, linked to various health issues including irritation, elevated blood pressure, and sleep disturbances (Abbasi *et al.*, 2019; Anjum, Kumari, 2022; Zare *et al.*, 2020; Kotus, Kostek, 2008). High-frequency noise can cause headaches, fatigue, and immune system suppression (Münzel *et al.*, 2018; Szychowska *et al.*, 2018; Anjum, Kumari, 2022), while residents near wind farms often experience annoyance, impacting their daily tasks (Pawlaczyk-Łuszczyńska *et al.*, 2014; Hafke-Dys *et al.*, 2016). Previous research indicates that individuals within a 500 m radius of wind energy plants exhibit significant responses to the turbine noise, with annoyance extending to 1900 m (van den Berg, 2004). However, further investigations are needed due to limited empirical data linking public annoyance directly to the wind turbine noise.

Wind turbine noise can be classified based on frequency as tonal or broadband, originating from aerodynamic or mechanical sources (Hansen, Hansen, 2020). Environmental factors such as temperature, humidity, and obstacles can affect noise propagation, with the turbine blade motion particularly noticeable at night (Deshmukh *et al.*, 2019; Nguyen *et al.*, 2020). To mitigate noise pollution, governmental guidelines specify maximum permissible noise levels, necessitating adherence to local factors during turbine deployment (Davy *et al.*, 2018; Gallo *et al.*, 2016).

Horizontal axis wind turbines (HAWTs) dominate wind energy extraction but face limitations such as size and maintenance requirements (Davy *et al.*, 2018; Gallo *et al.*, 2016). In contrast, vertical axis wind turbines (VAWTs) offer reduced mechanical noise transmission and diminished aerodynamic noise levels (Möllerström *et al.*, 2014; Graham, Pearson, 2022). However, research on VAWTs remains somewhat limited, prompting a need for comprehensive evaluations to optimize efficiency while minimizing noise disruption (Dumitrescu *et al.*, 2010; Iida *et al.*, 2004).

The Savonius VAWT (SVAWT) emerges as a promising option due to its reduced noise emission and suitability for urban environments (Akwa *et al.*, 2012; Doerffer *et al.*, 2021). Despite producing less noise than HAWTs, the trade-off for noise reduction leads to a decreased energy output (Oerlemans, Fuglsang, 2012; Ghasemian, Nejat, 2015). Enhancements such as rotor segmentation have been proposed to improve efficiency (Kacprzak *et al.*, 2013; Mahmoud *et al.*, 2012; Sun *et al.*, 2012; Driss *et al.*, 2014).

Research in wind energy has shifted towards urban integration and regulatory compliance, driven by environmental concerns (New World Wind, n.d.; IBIS Power, n.d.). Nevertheless, a detailed analysis of the VAWT power production and acoustics remains lacking (Akwa *et al.*, 2012; Sachar *et al.*, 2023; Jeong *et al.*, 2014). Thus, evaluating Savonius VAWTs for urban environments, considering noise-efficiency trade-offs, is crucial for public acceptance (New World Wind, n.d.; IBIS Power, n.d.). This study aims to address this gap by conducting experiments on a standard Savonius rotor, exploring the impact of segmentation and assessing the sound quality (Fastl *et al.*, 2007).

2. Wind turbine model and experimental setup

Various configurations of the Savonius rotor were devised and tested for the research detailed in this paper, with wind velocities ranging from 7 m/s to 12 m/s. The experimentation was conducted within a dedicated test section, depicted in Fig. 1, established at the Institute of Fluid Flow Machinery Polish Academy of Sciences (IMP PAN). This facility comprises three inlet fans capable of operating at adjustable speeds. A wind velocity of 8.5 m/s was maintained for the investigations reported herein.

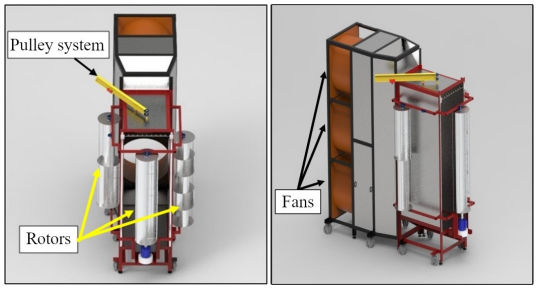

Fig. 1. Test section used in experiments.

The calibration of the test stand posed a challenge in achieving uniformity in the outlet stream. Three streams from propulsion fans were uniformly distributed by changing the local density of meshes at the screen between fans and the test section. An adequate location of one-, two-, and three-layers of meshes allowed obtaining a satisfactory uniformity of the outlet stream. On top of that a honeycomb straightener was inserted to reduce the transversal fluctuations in the air stream. The velocity was measured at the measurement points forming a grid with a spacing of 100 mm to confirm the uniformity of the outlet stream. This was obtained with the help of a support line holding nine Prandtl probes across the stream as shown in Fig. 3. It was measured that the standard deviation of the outlet velocity was around 10 %. This uniformity of the incoming stream was satisfactory in such a simple test stand. As shown in Fig. 3, a Prandtl probe is mounted in the middle of the outlet box to provide a reference stream velocity.

The test section can operate one rotor at any given time, while it can accommodate the simultaneous mounting of three distinct rotors for storage purposes (Fig. 1). Additionally, a pulley system facilitates the manipulation of these rotors. The three rotor configurations utilized in this study include single-, double-, and five-segment variants, each with a height of 2.2 m and a diameter (D) of 0.5 m. An integral feature of the test section is its loading apparatus, enabling the modification of the load exerted on the tested rotors. This functionality allows for a comparative analysis under various loading conditions, with concurrent noise measurements captured via microphones. Specifically, this study focuses on a comparison between single and five-segment rotor configurations. The single-segment rotor mirrors the conventional Savonius rotor design, comprising 'S'-shaped buckets spanning between two end plates at a height denoted as 'H'. In contrast, the five-segment rotor configuration consists of five rotors of identical height stacked atop one another, each rotated at 90° relative to the preceding segment orientation. This arrangement is illustrated in Fig. 2.

The measurement scenario consisted of quantifying the performance of the two wind turbines at their complete operational TSR range. The noise emissions were mainly focused on four cases:

- stopped rotor at different wind speeds;
- no-load condition/free run: the load is being withdrawn and the rotor is at its maximum speed of rotation at any given wind speed;
- loaded condition: rotor working under different load conditions;
- the background noise consisted only of the test section in the lab (without a rotor).

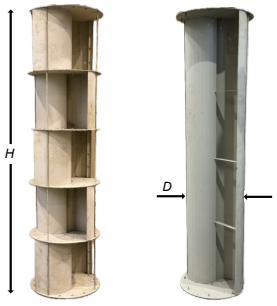

Fig. 2. a) Five-segment rotor; b) single-segment rotor.

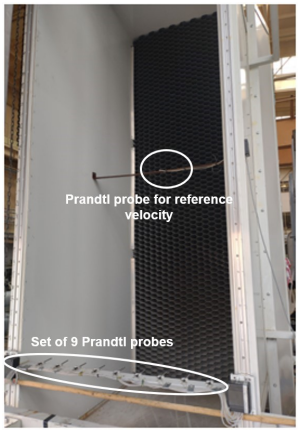

Fig. 3. Test section stream outlet.

The experiment involved both rotors, with a microphone positioned as depicted in Fig. 4. The microphone location is indicated by the red ellipse. It is placed at the same location for all the tests carried out. The microphone is located in the middle of the test section outlet in the vertical direction. In the horizontal direction, it is placed outside the stream leaving the test section. It is at a distance of 0.28 m away from the test section outlet plane, making sure that the microphone is sheltered from the air jet.

At the jet outlet the static pressure is the same as the ambient pressure, therefore one may assume that the free shear layer generated downstream of the test section wall should follow the wall direction. Such a free shear layer starts at the test section outlet and expands with the angle of ±7° due to turbulent mixing. This is indicated in Fig. 5a showing that the shear layer is far away from the microphone location.

The presence of the rotor close to the outlet plane may impose further deflection of this shear layer. In order to make sure that the rotor does not enforce the interaction of the shear layer with microphone, the numerical simulations for the investigated configuration have been carried out. This simulations have been done for the two limiting cases: no-load (TSR = 1.8) and maximum-load (TSR = 0.9).

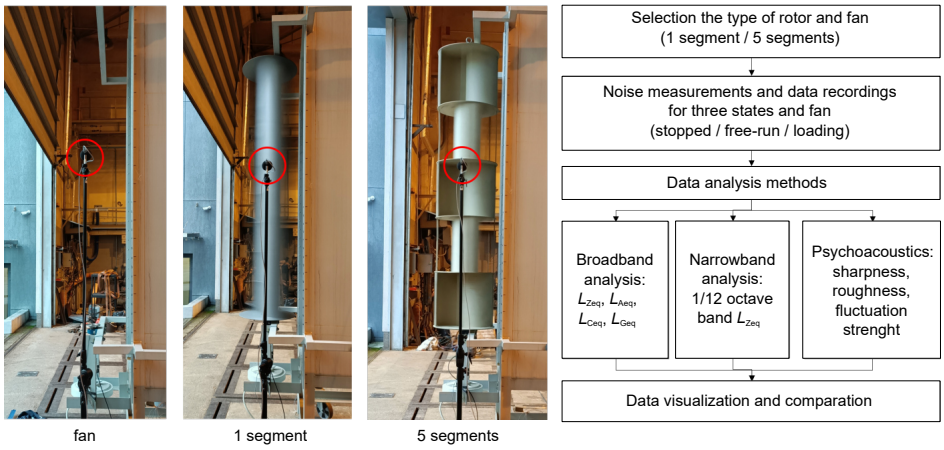

Fig. 4. Noise measurement setup and block diagram of the measurement procedure.

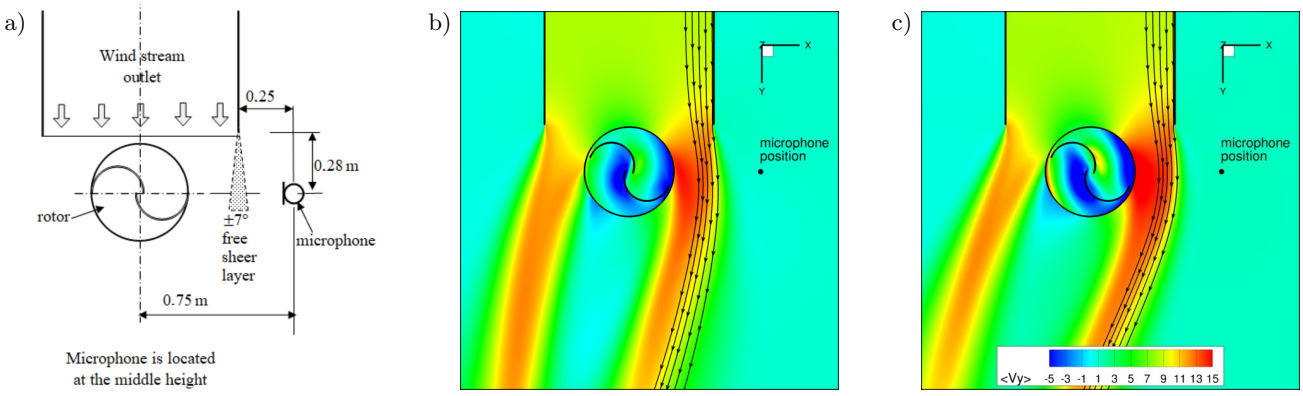

Fig. 5. Acoustic measurement setup: a) test section outlet configuration; b) CFD of the outlet flow TSR = 0.9; c) CFD of the outlet flow TSR = 1.8.

Numerical simulations were performed using the FINE/Open NUMECA/CADENCE software, which employs a finite volume method with a central differencing scheme enhanced by artificial dissipation for spatial discretization, and a Runge–Kutta type time integration scheme. The time step in each case corresponds to a rotor rotation of 2°. A full multigrid strategy was applied to enhance the convergence rate. The calculations were carried out under the assumption of a two-dimensional, incompressible, and turbulent flow (at the mid-span of the wind tunnel), using the k-ω SST turbulence model. Boundary conditions were defined based on the values measured on the experimental setup. To allow for the full development of the flow, simulations were conducted over 20 full revolutions. The computations were then continued for an additional 10 revolutions, over which the results were time-averaged. The results of the numerical simulations, presented in Figs. 5b and 5c, were obtained based on experience with unsteady flow configurations including aeroacoustic effects (Flaszynski *et al.*, 2021; Grzelak *et al.*, 2024; Suresh *et al.*, 2024). In Figs. 5b and 5c, the time-averaged velocity (over 10 rotations) is shown. These results indicate that the free shear layer developing downstream of the wind tunnel wall is far from the microphone location. The induced air flow around the microphone is of very low velocity, confirming that the jet downstream of the wind tunnel does not affect microphone recordings.

The objective of the tests was to assess the overall noise generated by the rotor under various loading conditions. Subsequently, the same procedure was repeated, with each rotor type subjected to identical operating conditions. Noise measurements were taken using a sampling method, employing a class 1 Sound Level Meter SVAN 979 with a high quality omnidirectional G.R.A.S. $^1/_2''$ measuring prepolarized free-field microphone, type 40AE and the SV 17 preamplifier. The sound level meter was calibrated before and after the measurements using the SV 36 acoustic calibrator. The raw sound data was recorded during the noise measurements for further analysis using the SVANPC++ software, version 3.4.4. Measurements were repeated three times for each case $N = 3$, with each sample recorded for T equal to 60 s. The measuring microphone was positioned using a tripod, halfway up the rotor, outside the mainstream from the test section exit, at a distance of 0.7 m from the rotor axis. A windscreen was used for the microphone.

Simultaneously, measurements were taken to determine the rotor performance characteristics and establish the relationship between the coefficient of power (C_p), TSR, and revolutions per minute (RPM). These experiments were conducted under conditions consistent with the noise measurements, with the fan frequency set to 35 Hz to produce a wind velocity of 8.5 m/s.

It is essential to note that the relative noise production discussed in this study between single and five-segment rotors does not fully represent the noise levels produced by rotors individually in real-world conditions, where factors such as inlet turbulence, temperature, humidity, and shear may significantly influence the noise levels.

The recorded acoustic data was analyzed using several methods, as shown in Fig. 4. First, the broadband analysis was performed. In this case the equivalent continuous sound pressure level (L_{eq}) for four weightings curves (Z, A, C, and G) was determined. Next, the analysis of the sound pressure level (SPL) was extended using a narrow band analysis. This analysis was performed using a $^1/_{12}$ octave band analyzer. The $^1/_{12}$ octave band equivalent SPL with the weighting curve Z was determined to evaluate the actual noise production between the considered rotors. The main aim of this analysis was to evaluate the actual noise production between the considered rotors. Those analyses were performed using the SVANPC++ software, version 3.4.4 and the Pulse Reflex software. The L_{eq}, for a given measurement period (T), was calculated using the selected weighting filter: Z, A, C, or G.

The indicator $L_{\mathrm{Zeq,Avg.}}(f)$ was computed for each $^1/_{12}$ octave band spectrum, and the average value was calculated as follows:

$$L_{\mathrm{Zeq,Avg.}}(f) = 10\log_{10}\left(\frac{1}{N}\sum_{i=1}^{N} 10^{L_{\mathrm{Zeq},T}(f)/10}\right)\ [\mathrm{db}], \quad (1)$$

where f is the frequency of the $^1/_{12}$ octave band, 180 filters were used for the frequency range from 0.71 Hz up to 22000 Hz, N is the number of recorded samples.

The third method was a psychoacoustic analysis. In this case selected metrics related to the sound quality such as sharpness, roughness, and fluctuation strength (FS) were determined. Sharpness is a hearing sensation related to frequency and independent of loudness. Sharpness corresponds to the sensation of a sharp, painful, high-frequency sound and is a comparison of the amount of high frequency energy to the total energy (Fastl, Zwicker, 2007). Roughness is a complex effect which quantifies the subjective perception of the rapid (15 Hz–300 Hz) amplitude modulation of a sound. The unit of measure is *asper*. One *asper* is defined as the roughness produced by a 1000 Hz tone of 60 dB which is a 100 % amplitude modulated at 70 Hz (Fastl, Zwicker, 2007; Cox, n.d.). The FS is similar in principle to roughness except that it quantifies a subjective perception of a slower (up to 20 Hz) amplitude modulation of a sound. The sensation of the FS persists up to 20 Hz, then at this point, the sensation of roughness takes over (Fastl, Zwicker, 2007; Cox, n.d.). The main purpose of this analysis was to extend the knowledge about phenomena related to the perception of the sound emitted by the examined rotors by human beings. A psychoacoustic

analysis was conducted using the Pulse Reflex software, version 21.0.0.567, provided by Bruel & Kjaer (Fastl, Zwicker, 2007).

For all types of the performed analysis, three independent recordings (independently for each rotor type and considered conditions), with T set to 60 s, were analyzed. Finally, the average value was calculated and presented.

3. Results and analysis

The findings from experiments conducted on a single- and five-segment rotor installed in the test section, as illustrated in Fig. 4, and operated at a wind speed of 8.5 m/s, are depicted in Fig. 6 (see Subsec. 3.2). This wind velocity, generated by the fans, corresponds to a frequency of 35 Hz and is denoted by a dashed vertical line in the plots. It is essential to acknowledge that the acoustic emissions from the fans were notably high. Therefore, the comparison between the two rotors should focus solely on the difference in the SPL, rather than absolute values.

The noise measurements were conducted under the three following conditions:

- rotor under the maximum-loading condition, where the single-segment rotor operated at 300 RPM (equivalent to a frequency of 5 Hz), and the five-segment rotor operated at 250 RPM (equivalent to a frequency of 4.17 Hz);
- rotor without loading, with the five-segment rotor operating at 500 RPM (equivalent to a frequency of approximately 8.5 Hz) and the single-segment rotor operating at 575 RPM (equivalent to a frequency of 9.55 Hz);
- test section with the rotor in a stationary (non-rotating) position.

The aforementioned conditions were applied to:

- the test section with the five-segment rotor;
- the test section with the single-segment rotor;
- the test section noise without a rotor (fan noise).

The obtained measurement data was used to perform 4 types of analysis. First, a broadband analysis was performed.

The effect of the rotor presence and the background noise of the test stand, generated mainly by the propulsion fans, is presented in Fig. 6a. The rotor type plays a minor role on the generated noise. Nevertheless, its implementation contributes significantly to the noise generated by the propulsion fans. However, this contribution takes place below the frequency of $f < 130$ Hz only.

The detailed results are shown in Subsec. 3.1. Next, the narrowband analysis is detailed in Subsec. 3.2. In Subsec. 3.3., the acoustic analysis was extended by the selected sound quality measures. Finally, a relation between the noise produced and the rotor efficiency is detailed in Subsec. 3.4.

3.1. Broadband analysis

The main aim of the broadband analysis was to show the total level of noise using three types of frequency weighting curves: A, C, Z. For better understanding of the considered phenomena, the broadband analysis was extended by a low frequency analysis, including infrasound, using the weighting curve G. The average equivalent SPL was calculated for this purpose for all the considered cases: stopped rotor, rotor with load (maximum-loading conditions), rotor without load (free-run). The fan noise (the noise level without a rotor) was used as a reference for the cases discussed, as seen in Fig. 6. The average values were calculated using three samples of equivalent sound pressure levels. Each sample value was calculated for 60-second sound recordings. The obtained results are shown in Table 1.

The detailed assessment of the noise level emitted by a rotor in the presented measuring setup is difficult for the following reasons: the used fan system produced a very high level of background noise; the noise emission from the rotating rotor is closely related to the wind speed; and the rotor is not a wind-independent source of the noise. For these reasons, the traditional method of evaluating acoustic emissions – measuring the noise immission and the acoustic background, then calculating the noise emission as the energy difference between them – is not appropriate. In the measurement system used, the rotor acts as a background noise modulator and, in selected situations, causes an increase in the noise level. The way in which the background noise is modulated is directly related to the design of the rotor and the way of its rotation, depending on the load. Taking this fact into account, it was proposed to assess the rotor noise using simply the difference between the noise level with the rotor (in a particular state) and the fan

Table 1. Comparison of sound levels for one-segment and five-segment rotors.

Measurement case	One-segment rotor				Five-segment rotor			
	L_{Aeq}	L_{Ceq}	L_{Zeq}	L_{Geq}	L_{Aeq}	L_{Ceq}	L_{Zeq}	L_{Geq}
Fan noise	95.7	101.9	102.0	82.8	95.7	101.9	102.0	82.8
Stopped rotor	96.2	102.1	102.4	88.2	95.7	101.9	102.2	89.8
Free run	99.0	105.3	109.3	117.1	95.7	102.3	103.3	98.5
Rotor with load	96.1	103.0	111.7	110.0	95.7	101.9	104.1	96.7

noise level. Based on this assumption, the difference levels were calculated for both the considered types of rotors. These calculations were done for two cases.

First, the difference between the emission and the background noise levels was determined. The result was marked using symbol Δ. The obtained results are shown in Table 2. Next, the difference between the rotors was calculated. The one-segment rotor values were used as a reference for this purpose. The results are shown in Table 3. The noise of the stopped rotor results from a static disturbance of the airflow. The noise level exceeding the background acoustic level results from the turbulence introduced by the rotor structure in the air stream because the rotor is stopped. For the single-segment rotor, higher noise levels were recorded for each indicator type (see Table 1). For the free-run mode for the single-segment rotor, the noise level was 3 dB higher compared to the acoustic background for curves A and C and by 7.3 dB for curve Z (see Table 2). For a five-segment rotor, the change in the acoustic background level is very small. An increase in the background noise level of 2.1 dB was noticeable only for the load mode and for the curve Z analysis. The greatest differences for the curve G were noticed between the fan noise and the added rotor. Placing the stopped rotor in the air flow increased the noise level by over 5 dB for the single-segment rotor and by over 7 dB for the five-segment rotor. This situation can be noticed in figures presented in Subsec. 3.2. In the free-run conditions for a single-segment rotor, the L_{Geq} level increased by over 34 dB compared to the level of the fan itself. The noise level for the five-segment rotor in the free-run conditions was 18.6 dB lower than for the single-segment rotor. In the load conditions, the noise level for the single-segment rotor decreased by 7.1 dB compared to the free-run conditions. In the case of the five-segment rotor, the difference between the noise level for the free-run and the load conditions was 1.8 dB. The noise level for the single-segment rotor in the load phase was over 13 dB higher compared to the noise level generated by the five-segment rotor.

An additional analysis involved determining the differences in the noise level between the single-segment rotor and the five-segment rotor. Even when the rotors were not rotating, the noise level was (slightly) higher for the single-segment rotor than for the five-segment rotor. The noise level for the single-segment rotor in the free-run mode was 3 dB higher than the acoustic background (for curves A and C) and 6 dB for curve Z. The difference between curves A, C, and Z is affected by the strong attenuation introduced by curves A and C for low frequency. The noise level for a single-segment rotor in the load mode was slightly higher for A- and C-corrected indicators and 7.6 dB higher for the curve Z. This means that the differences between the rotors occur mainly in the low-frequency range, with higher levels recorded for the single-segment rotor. Based on the research, it has been found that a single-segment rotor causes a greater increase in the background noise level than a five-segment rotor, and a single-segment rotor causes a measurable increase in the acoustic background level, especially for the free run mode and weighting curves A and C. A loaded single-segment rotor causes only a slight increase in the acoustic background level for weighting curves A and C. The greatest increase in the noise level was recorded for the correction curve Z, especially for the loaded single-segment rotor. The five-segment rotor did not cause any significant change in the acoustic background level for the weighting curves A and C. A slight increase in the level was noted only for the load mode and the curve Z. In practice, this means that a five-segment rotor will be less noticeable (in the acoustic field) than a single-segment rotor. Its design ensures that the acoustic background level does not change during its operation.

Based on the broadband analysis, it was found for the curve G that the greatest differences in the noise emission, regardless of the rotor type, occurred for the indicator corrected by the weighting curve G. This clearly indicates a low-frequency type of emission. More detailed considerations regarding the distribution of acoustic energy in the frequency domain are presented in Subsec. 3.2. Quantitatively, it has been shown that low-frequency noise emissions, expressed by the indicator L_{Geq}, for a single-segment rotor are many times higher than for a five-segment rotor. The single-segment rotor in the free-run phase, under the given test conditions, emitted energy nearly 73 times higher than the five-segment rotor. In the load conditions, the acoustic energy emitted by the single-segment rotor was 21 times higher than the acoustic energy emitted by the five-segment rotor. Therefore, the working conditions had a significant impact on the level of emissions. Low-frequency emissions were the highest in the free-run phase. The results obtained have considerable practical significance. First of all, they indicate that the problem of noise emissions con-

Table 2. Noise difference analysis results calculated in relation to fan noise.

Measurement case	One-segment rotor				Five-segment rotor			
	ΔL_{Aeq}	ΔL_{Ceq}	ΔL_{Zeq}	ΔL_{Geq}	ΔL_{Aeq}	ΔL_{Ceq}	ΔL_{Zeq}	ΔL_{Geq}
Stopped rotor	0.6	0.2	0.4	5.4	0.0	0.0	0.2	7.1
Free-run	3.3	3.4	7.3	34.3	0.0	0.4	1.3	15.7
Rotor with load	0.4	1.1	9.7	27.2	0.0	0.0	2.1	13.9

cerns low frequencies. The design of the rotor significantly affects noise emissions. The five-segment rotor is characterized by significantly lower acoustic energy emissions, regardless of the operating conditions. The biggest differences occurred in the free-run phase. To extend the analysis, calculations were performed using sound quality measures. Indicators sensitive to signal modulation, such as roughness and the FS, are of particular importance. The results of this study are shown in Subsec. 3.3.

Table 3. Noise difference analysis between rotors*.

Measurement case	Indicator type			
	ΔL_{Aeq}	ΔL_{Ceq}	ΔL_{Zeq}	ΔL_{Geq}
Stopped rotor	0.6	0.2	0.2	–1.6
Free-run	3.3	3.1	6.0	18.6
Rotor with load	0.4	1.1	7.6	13.3

*positive value: the single-segment rotor produced a greater SPL; negative value: the five-segment rotor produced a greater SPL.

3.2. Narrowband analysis

In this section, the narrowband analysis results are presented. As mentioned before, the narrowband analysis was performed using a constant percentage bandwidth analyzer with a 1/12 octave band resolution. The results are presented in two groups of figures: first separated for the considered state (Fig. 6), second separated for the considered rotors (Fig. 7).

As depicted in Fig. 6a, both rotors exhibit similar noise level outputs when the rotor is stationary, allowing for a direct comparison under both no-load and loaded conditions (Figs. 6b and 6c). Notably, the angular position of the stopped rotor relative to the wind direction did not influence the results. The RPM of the rotors were standardized as the reference value for each scenario, with the corresponding frequencies and recorded sound energy levels [dB].

Distinct differences in the acoustic energy distribution among the considered rotors are observable, particularly at low frequencies, notably between 1 Hz and 51 Hz, as illustrated in Figs. 6b and 6c. A significant disparity in both frequency and acoustic energy production within this range is evident (as was mentioned in the previous section, especially for the weighting curve G). Consequently, the collective SPL for this frequency band was computed. An analysis of the entire frequency spectrum reveals discrepancies not only in the low-frequency range but also around 1000 Hz. Specifically, the single-segment rotor generated higher sound levels than the five-segment rotor, particularly under no-load conditions (Fig. 6c). For loaded conditions, differences are primarily observed in the low-frequency range, leading to analysis limited to frequencies between 1 Hz to 51 Hz (Fig. 6b).

The initial peak corresponds to a weak impulse frequency of approximately 4.8 Hz when maximum-

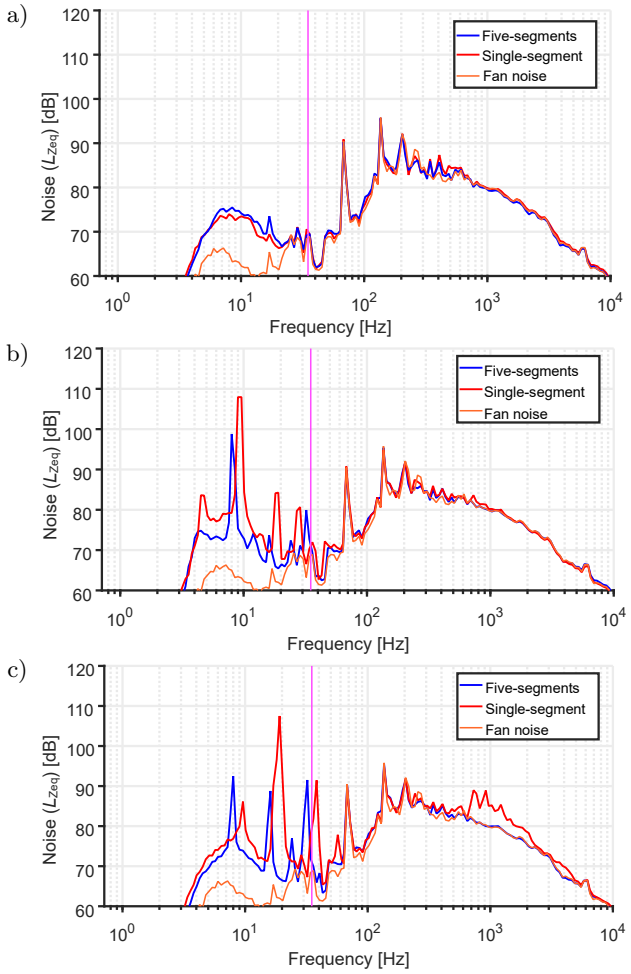

Fig. 6. 1/12 octave bands spectrum for examined rotors presented separately for considered conditions: a) stopped rotor; b) rotor with load; c) rotor without load (free-run).

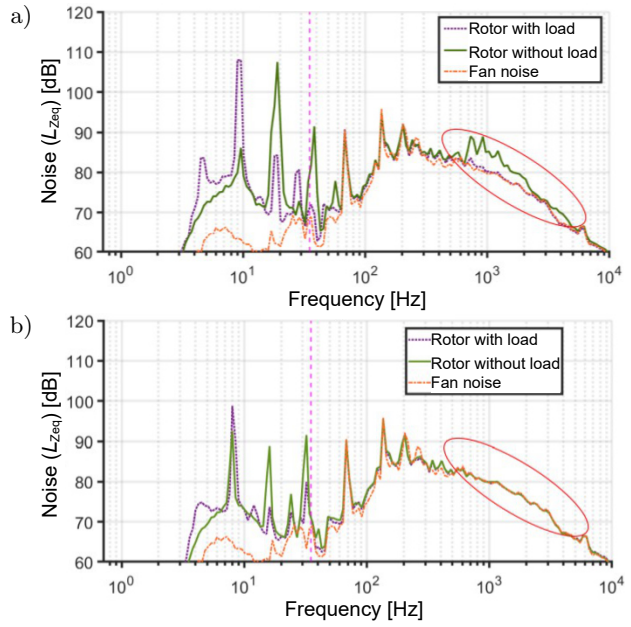

Fig. 7. 1/12 octave bands spectrum for considered conditions presented separately for examined rotors: a) single-segment rotor; b) five-segment rotor.

loading is applied, aligning with the complete rotor RPM of 286 (4.78 Hz). This phenomenon is also evident in unloaded conditions. Additionally, the effect of two blades is apparent in both scenarios, corresponding to an RPM value of 572 (9.55 Hz), indicating a doubling of the frequency relative to the RPM. Notably, low-frequency, narrow-band rotational components typically occur at the blade passage frequency (the rotational speed multiplied by the number of blades) and its integer multiples, consistent with the findings presented in (Pearson, Graham, 2014). Mathematically, the acoustic energy for all sub-bands needs to be summed from 1 Hz to 51 Hz. Specifically, 75 sub-bands are present from 0.71 Hz up to 51 Hz. A unified value for this frequency range was computed. Initially, the SPL is converted to a relative exposure, representing the square of the acoustic pressure divided by the square acoustic reference pressure, for each considered sub-band using the equation:

$$Ex = 10^{(l/10)},$$

where Ex denotes the relative exposure and l represents the SPL expressed [dB]. Subsequently, these values are aggregated. Finally, the sum of the relative exposure is transformed to the SPL using logarithms via the equation:

$$L = 10 * \log 10(\mathrm{sum}(Ex)).$$

The discrepancy between the rotors was subsequently determined: this difference = −1 dB for stationary rotors, indicating a nearly identical SPL for these conditions; for rotors under no-loading, this difference = 11.2, signifying that the single-segment rotor generated an SPL 11.2 dB higher than the five-segment rotor. Hence, it can also be inferred that the acoustic energy produced by the single-segment rotor is 13.3 times greater than that of the five-segment rotor. A comparable difference of 11.4 is observed for the loaded rotor. In this instance, the acoustic energy produced by the single-segment rotor is 13.8 times greater than that of its five-segment counterpart.

As previously mentioned, an elevation in the noise produced by the single-segment rotor is noted, between approximately 500 Hz and 1500 Hz. This region is delineated by a red ellipse in Fig. 7a and is absent in the case of its five-segment counterpart. Additionally, it was observed that noise peaks in the case of a five-segment rotor transitioned towards broadband frequencies and attenuated at a faster rate. This phenomenon arises from the heightened mixing of complex vortices formed in the case of a five-segment rotor compared to two rotors under similar testing conditions, disrupting the coherence patterns. This effect, akin to the addition of serrations in aircraft wings, serves to distribute noise-generating vortices, consequently reducing noise levels (Moreau, Doolan, 2013; van der Velden, Oerlemans, 2017; Mathew *et al.*, 2016; Oerlemans *et al.*, 2009). This observation elucidates the acoustic energy distribution presented in Fig. 7, where identical frequencies are recorded with varying sound levels for each scenario.

Upon evaluation of both cases, it becomes apparent that the unloaded rotor generates more noise compared to its loaded counterpart, as depicted in Fig. 7. It is evident from the plots and tables that the five-segment rotor yields a lower sound energy compared to its single-segment counterpart, a conclusion further validated by calculating the sound intensity difference between the two cases.

3.3. Psychoacoustics

For the next part of the research, psycho-acoustics related to sound quality was analyzed based on the studies presented in (Sahai, 2016; Blauert, 2005). Figure 8 shows a variation in the different sound parameters under consideration. The FS, representing the modulation in sound, is at its peak value for a frequency of about 4 Hz.

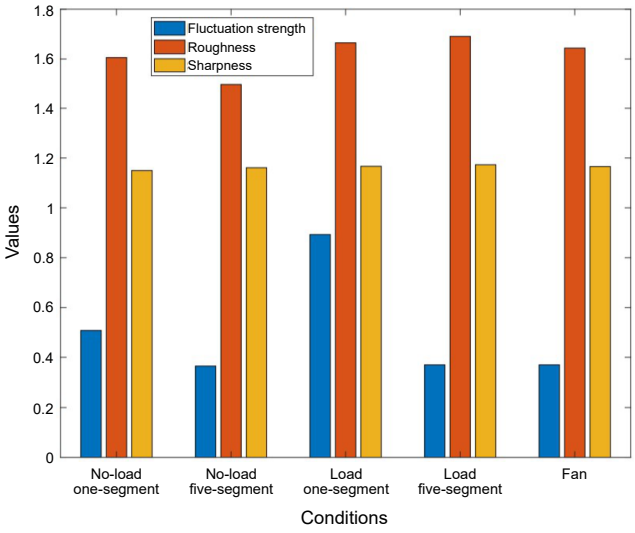

Fig. 8. Information about sound quality for single and five-segment rotor under different operational conditions, the units are as follows: FS [vacil], roughness [*asper*], sharpness [acum].

A higher FS draws more attention to it and can thus cause more irritation. It is evident from Fig. 6b that a peak related to the BPF (blade passing frequency) takes place about this frequency for the case when the rotor is under maximum-loading. This is also seen in Fig. 8. Another factor under consideration is the sound roughness which reaches a maximum at a frequency of about 70 Hz. As anticipated from the power spectrum plots, sharpness, which is related to how pleasant one feels when hearing the noise, is mainly dominated by higher frequencies and is similar in all the cases.

A broadband analysis of selected SQ parameters showed that it was the FS that was the metrics distinguishing the examined rotor types. Differences in the FS parameter values occurred both in the free-run (slight differences) and the load mode (larger changes). An extended analysis of this indicator in the frequency domain was performed to more precisely check the properties of the tested rotors in terms of diversity in the FS parameter. Due to the fact that SQ measures refer to perceptual phenomena, the FS spectrum is presented on the Bark scale. The analyses were performed for a free run and load phases. The obtained results are shown in Fig. 9. A higher value of the FS indicator (related to the five-segment rotor) in the free run mode for a single-segment rotor occurred for the frequency bands covering the Bark scale from 5 to 8 (the widest range), 11–13, and 17–19. A slight increase in the FS index was noted only for the 3-Bark band in the load phase of the five-segment rotor. It can be summarized that the FS in this rotor type does not depend on the type of rotation and that this rotor type does not induce this type of sensation. In the case of a single-segment rotor, a drastic increase in the FS value was observed in the load conditions. Moreover, a significant increase in the number of bands in which an increase in the FS took place was also observed. The lower range was expanded by a band of Bark 3. The two higher sub-ranges were merged into one range from 10 to 17 Barks. This means that the impression of the modulation strength expanded in the frequency domain, taking on a broadband character and its strength increased significantly.

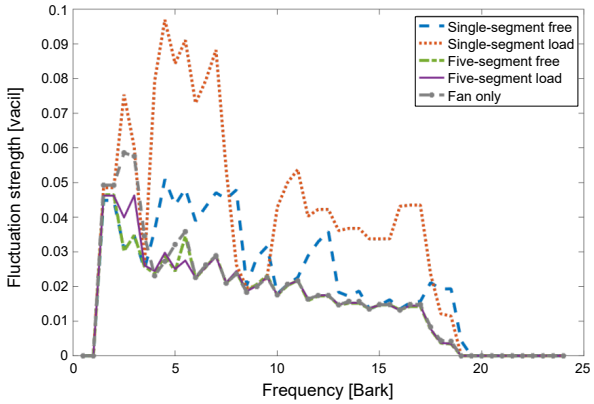

Fig. 9. FS spectrum on the Bark scale for examined rotors under considered conditions.

A single-segment rotor modulates background noise much more effectively. This results directly from its design. The wide blade of the wing captures a large volume of air at a given moment (which is the center of acoustic wave propagation), causing instantaneous rapid changes in the sound pressure (resulting from the rotor rotational speed), which is audible as a noise modulator (a sound similar to a flag flapping or flapping in the wind). This was confirmed by a higher value of the FS index for a single-segment rotor. The modulation of the background noise in a five-segment rotor is very low, and the obtained indicators do not differ significantly from the values obtained for the background noise. Less disturbance of the acoustic background for a five-segment rotor comes at the cost of a lower energy efficiency of this structure. A single-segment rotor is characterized by greater efficiency and more noticeable changes in the acoustic background. The broadband SQ results presented for the fan only, especially the FS, obtained for the fan noise (without rotors), have similar values as the stopped rotors and the five-segment rotor with load.

The frequency domain analysis of the fan noise (without rotors) indicated that the FS distribution was similar to the five-segment rotor (for both conditions: free run and load) and was even greater for Bark 2–4 than for this rotor. It means that the five-segment rotor efficiently reduced the modulation of the sound.

3.4. Rotor efficiency and noise

The final finding, which explores the impact of segmentation on efficiency alongside noise, is illustrated in Fig. 10. The performance variation across the entire operational range of TSR has been depicted. Notably, the single-segment rotor exhibits superior C_p values throughout the TSR range under examination. It should also be noted that the maximum efficiency can be seen at a TSR value of about 1 for both cases, corresponding to a rotor rotational speed of 300 RPM. The maximum rotational speed in the no-load case takes place just above 500 RPM. A single-segment rotor achieves a maximum efficiency of 33.15 %, whereas a five-segment rotor attains a maximum efficiency of 26.45 %. A relative decrease of 20 % in efficiency is observed for a segmented rotor compared to a conventional Savonius rotor.

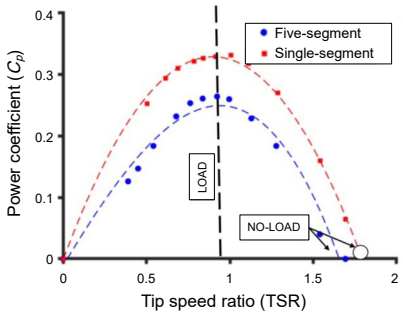

Fig. 10. Performance characteristics with respect to TSR.

Additional plates are inserted in the case of a segmented rotor (Fig. 2). These plates introduce additional surfaces at which boundary layers are formed, inducing viscous losses in the rotor. In addition, these boundary layers are inserted into the highly curved

blades, which generate a pressure gradient normal to the blade surface. Such a pressure gradient generates a transverse flow within the boundary layer, becoming a source of 3D flow structures. These two reasons become a source of increased losses at a segmented rotor.

Comparing these results to the SPL analysis presented in Subsec. 3.2, it should be recalled that the SPL in stopped rotors (RPM = 0) is nearly the same. In the case of maximum-loading rotors, the single-segment rotor produces a much higher SPL than the five-segment rotor. It should be taken into account that the introduction of additional plates in the segmented rotor becomes a source of streamwise vorticity, which is intersecting blade span-wise vortices. This vortex disintegration mechanism reduces noise but often increases losses. This may also shift the emitted noise from low to higher frequencies. The differences occur mainly in the low-frequency region (1 Hz–51 Hz). Thus, it can be concluded that an increase in power production is redeemed at the expense of an increase in noise emissions. The contribution of noise emissions from a single-segment in the free-run condition of the rotor is still higher and includes contributions from higher frequencies (around 1000 Hz), as well.

4. Conclusions

The presented study indicates that the noise produced by a wind turbine is influenced by its operational parameters. This research involves a comparative analysis between a single-segment rotor and a five-segment rotor, offering insights into the most favorable operating conditions and the rotor type that minimizes the noise while maximizing the efficiency. It can be inferred from the results obtained that:

- a five-segment rotor produces less overall acoustic energy as compared to that produced by a single-segment rotor. The changing phase of the segments breaks the coherence of the flow and shifts the noise energy content to higher frequency spectra, where the dissipation rate is faster;
- the amount of acoustic energy produced decreases as the load increases, peaking when the rotor is spinning without any external-load;
- the greatest differences in noise emissions between the considered types of rotors concern low frequency noise.
- under the specified test conditions at a wind speed of 8.5 m/s, a single-segment rotor demonstrates a greater efficiency compared to a five-segment rotor, achieving a maximum performance efficiency of 32 % as opposed to 26.5 % for the five-segment rotor;
- following the conclusions, the sound quality of a five-segment rotor makes it a preferable choice.

Very practical conclusions can be drawn from the analysis: if the lowest possible noise level is a critical parameter in a given area, it is recommended that multi-segment structures are used. However, if the priority is to obtain the highest possible efficiency of the system, then the first choice will be to use single-segment systems.

The analysis of the sound quality measures indicated that the metrics such as roughness and sharpness are similar for both rotors. The significant differences between the examined rotors were noticed in the FS. The greater value of these metrics occurred for the single-segment rotor. The SQ metric values in the case of the five-segment rotor were similar in all conditions (free-run and with load) to the values obtained for the fan noise. Further analysis is required in a quieter environment to maintain the efficiency of the single-segment rotor with low noise levels. An experimental campaign has been planned in collaboration with the Technical University of Delft to localize the noise sources using a microphone array in contrast to a single microphone used for this study. This will help in optimizing the design and reaching our final aim of more production of power with less noise disturbance.

Funding

The project received funding from the European Union's Horizon 2020 research and innovation programme under the Marie Skłodowska-Curie grant agreement no. 860101-zEPHYR and was supported by CI TASK (Gdańsk, Poland).

References

1. Abbasi M. *et al.* (2019), Assessment of role of job components and individual parameters on the raised blood pressure in a noisy industry, *Archives of Acoustics*, **44**(3): 575–584, https://doi.org/10.24425/aoa.2019.129272.
2. Akwa J.V., Vielmo H.A., Petry A.P. (2012), A review on the performance of Savonius wind turbines, *Renewable and Sustainable Energy Reviews*, **16**(5): 3054–3064, https://doi.org/10.1016/j.rser.2012.02.056.
3. Anjum S., Kumari A. (2022), Evaluation of noise pollution in Bengaluru City, India during COVID-19 pandemic, *Archives of Acoustics*, **47**(2): 131–140, https://doi.org/10.24425/aoa.2022.141644.
4. Blauert J. (2005), *Communication Acoustics*, Springer, https://doi.org/10.1007/b139075.
5. Cox T. (n.d.), Roughness – Fluctuation Strength, https://hub.salford.ac.uk/sirc-acoustics/psychoacoustics/sound-quality-making-products-sound-better/an-introduction-to-sound-quality-testing/roughness-fluctuation-strength/ (access: 27.03.2024).
6. Davy J.L., Burgemeister K., Hillman D. (2018), Wind turbine sound limits: Current status and recommendations based on mitigating noise annoyance,

Applied Acoustics, **140**: 288–295, https://doi.org/10.1016/j.apacoust.2018.06.009.

7. Deshmukh S., Bhattacharya S., Jain A., Paul A.R. (2019), Wind turbine noise and its mitigation techniques: A review, *Energy Procedia*, **160**: 633–640, https://doi.org/10.1016/j.egypro.2019.02.215.
8. Doerffer K., Telega J., Doerffer P., Hercel P., Tomporowski A. (2021), Dependence of power characteristics on Savonius rotor segmentation, *Energies*, **14**(10): 2912, https://doi.org/10.3390/en14102912.
9. Driss Z., Mlayeh O., Driss D., Maaloul M., Abid M.S. (2014), Numerical simulation and experimental validation of the turbulent flow around a small incurved Savonius wind rotor, *Energy*, **74**: 506–517, https://doi.org/10.1016/j.energy.2014.07.016.
10. Dumitrescu H., Cardos V., Dumitrache A., Frunzulică F. (2010), Low-frequency noise prediction of vertical axis wind turbines, [in:] *Proceedings of the Romanian Academy – Series A: Mathematics, Physics, Technical Sciences, Information Science*, **11**(1): 47–54.
11. Fastl H., Zwicker E. (2007), *Psychoacoustics: Facts and Models*, Springer Berlin, Heidelberg, 3rd ed., pp. 203–238, https://doi.org/10.1007/978-3-540-68888-4.
12. Flaszynski P., Piotrowicz M., Bacci T. (2021), Clocking and potential effects in combustor–turbine stator interactions, *Aerospace*, **8**(10): 285, https://doi.org/10.3390/aerospace8100285.
13. Gallo P., Fredianelli L., Palazzuoli D., Licitra G., Fidecaro F. (2016), A procedure for the assessment of wind turbine noise, *Applied Acoustics*, **114**: 213–217, https://doi.org/10.1016/j.apacoust.2016.07.025.
14. Ghasemian M., Nejat A. (2015), Aerodynamic noise prediction of a horizontal axis wind turbine using improved delayed detached Eddy simulation and acoustic analogy, *Energy Conversion and Management*, **99**: 210–220, https://doi.org/10.1016/j.enconman.2015.04.011.
15. Graham W., Pearson C. (2022), Noise from a model-scale vertical-axis wind turbine, *AIAA Journal*, **60**(1): 224–235, https://doi.org/10.2514/1.J060531.
16. Grzelak J., Carrillo L. G., Nakielski J., Piotrowicz M., Doerffer K. (2024), An innovative floating system with a Savonius rotor as a horizontal-axis wind turbine, *Polish Maritime Research*, **31**(2): 13–19, https://doi.org/10.2478/pomr-2024-0017.
17. Hafke-Dys H.Z., Preis A., Kaczmarek T., Biniakowski A., Kleka P. (2016), Noise annoyance caused by amplitude modulated sounds resembling the main characteristics of temporal wind turbine noise, *Archives of Acoustics,* **41**(2): 221–232, https://doi.org/10.1515/aoa-2016-0022.
18. Hansen C., Hansen K. (2020), Recent advances in wind turbine noise research, *Acoustics*, **2**(1): 172–207, https://doi.org/10.3390/acoustics2010013.
19. IBIS Power (n.d.), Complicated sustainability issues in real estate, solved beautifully and easily, https://www.ibispower.eu/powernest (access: 27.03.2024).
20. Iida A., Mizuno A., Fukudome K. (2004), Numerical simulation of aerodynamic noise radiated form vertical axis wind turbines, [in:] *Proceedings of the 18 International Congress on Acoustics.*
21. Jeong M.-S., Kim S.-W., Lee I., Yoo S.-J., Park K.C. (2014), Investigation of wake effects on aeroelastic responses of horizontal-axis wind-turbines, *AIAA Journal*, **52**(6): 1133–1144, https://doi.org/10.2514/1.J051899.
22. Kacprzak K., Liskiewicz G., Sobczak K. (2013), Numerical investigation of conventional and modified Savonius wind turbines, *Renewable Energy*, **60**: 578–585, https://doi.org/10.1016/j.renene.2013.06.009.
23. Kotus J., Kostek B. (2008), The noise-induced harmful effect assessment based on the properties of the human hearing system, *Archives of Acoustics*, **33**(4): 435–440.
24. Mahmoud N., El-Haroun A.A., Wahba E., Nasef M.H. (2012), An experimental study on improvement of Savonius rotor performance, *Alexandria Engineering Journal*, **51**(1): 19–25, https://doi.org/10.1016/j.aej.2012.07.003.
25. Mathew J., Singh A., Madsen J., Arce León C. (2016), Serration design methodology for wind turbine noise reduction, *Journal of Physics: Conference Series*, **753**(2): 022019, https://doi.org/10.1088/1742-6596/753/2/022019.
26. Möllerström E., Larsson S., Ottermo F., Hylander J., Bååth L. (2014), Noise propagation from a vertical axis wind turbine, [in:] *Proceedings of 43rd International Congress on Noise Control Engineering: Internoise 2014*.
27. Moreau D.J., Doolan C.J. (2013), Noise-reduction mechanism of a flat-plate serrated trailing edge, *AIAA Journal*, **51**(10): 2513–2522, https://doi.org/10.2514/1.J052436.
28. Münzel T., Schmidt F.P., Steven S., Herzog J., Daiber A., Sørensen M. (2018), Environmental noise and the cardiovascular system, *Journal of the American College of Cardiology*, **71**(6): 688–697, https://doi.org/10.1016/j.jacc.2017.12.015.
29. New World Wind (n.d.), WindTree, https://www.newworldwind.com/windtree (accessed: 27.03.2024).
30. Nguyen D.P., Hansen K., Zajamsek B., Catcheside P. (2020), Evaluation of wind farm noise amplitude modulation synthesis quality, *Applied Acoustics*, **166**: 107349, https://doi.org/10.1016/j.apacoust.2020.107349.
31. Oerlemans S., Fuglsang P. (2012), Low-noise wind turbine design, Siemens AG, https://www.ewea.org/events/workshops/wp-content/uploads/2012/12/EWEA-Noise-Workshop-Oxford-2012-1-1-Stefan-Oerlemans.pdf (access: 27.03.2024).
32. Oerlemans S., Fisher M., Maeder T., Kögler K. (2009), Reduction of wind turbine noise using optimized airfoils and trailing-edge serrations, *AIAA Journal*, **47**(6): 1470–1481, https://doi.org/10.2514/1.38888.

33. Pawlaczyk-Łuszczyńska M., Dudarewicz A., Zaborowski K., Zamojska-Daniszewska M., Waszkowska M. (2014), Annoyance related to wind turbine noise, *Archives of Acoustics*, **39**(1): 89–102, https://doi.org/10.2478/aoa-2014-0010.

34. Pearson C.E., Graham W.R. (2014), Experimental characterization of vertical-axis wind turbine noise, *The Journal of the Acoustical Society of America*, **137**(1): EL111–EL116, https://doi.org/10.1121/1.4904915.

35. Sachar S., Doerffer P., Flaszynski P., Kotus J., Doerffer K., Grzelak J. (2023), Correlation between the generated noise and effectiveness for a vertical axis Savonius type rotor, [in:] *AIAA SCITECH 2023 Forum*, https://doi.org/10.2514/6.2023-0611.

36. Sahai A.K. (2016), Consideration of aircraft noise annoyance during conceptual aircraft design, Ph.D. Thesis, RWTH Aachen University.

37. Sun X., Luo D., Huang D., Wu G. (2012), Numerical study on coupling effects among multiple Savonius turbines, *Journal of Renewable and Sustainable Energy*, **4**(5): 053107, https://doi.org/10.1063/1.4754438.

38. Suresh T., Flaszynski P., Carpio A.R., Kurowski M., Piotrowicz M., Szulc O. (2024), Aeroacoustic effect of boundary layer separation control by rod vortex generators on the DU96-W-180 airfoil, *Journal of Fluids and Structures*, **127**: 104133, https://doi.org/10.1016/j.jfluidstructs.2024.104133.

39. Szychowska M., Hafke-Dys H., Preis A., Kociński J., Kleka P. (2018), The influence of audio-visual interactions on the annoyance ratings for wind turbines, *Applied Acoustics*, **129**: 190–203, https://doi.org/10.1016/j.apacoust.2017.08.003.

40. van den Berg G. (2004), Effects of the wind profile at night on wind turbine sound, *Journal of Sound and Vibration*, **277**(4–5): 955–970, https://doi.org/10.1016/j.jsv.2003.09.050.

41. van der Velden W.C., Oerlemans S. (2017), Numerical study on combed teeth serrations for wind turbine noise reduction, [in:] *23rd AIAA/CEAS Aeroacoustics Conference,* https://doi.org/10.2514/6.2017-4172.

42. Zare S., Ghotbiravandi M.R., Elahishirvan H., Ahsaeed M.G., Rostami M., Esmaeili R. (2020), Modeling and predicting the changes in hearing loss of workers with the use of a neural network data mining algorithm: A field study, *Archives of Acoustics*, **45**(2): 303–311, https://doi.org/10.24425/aoa.2020.133150.